Electronic Supplementary Material (ESI) for Integrative Biology.

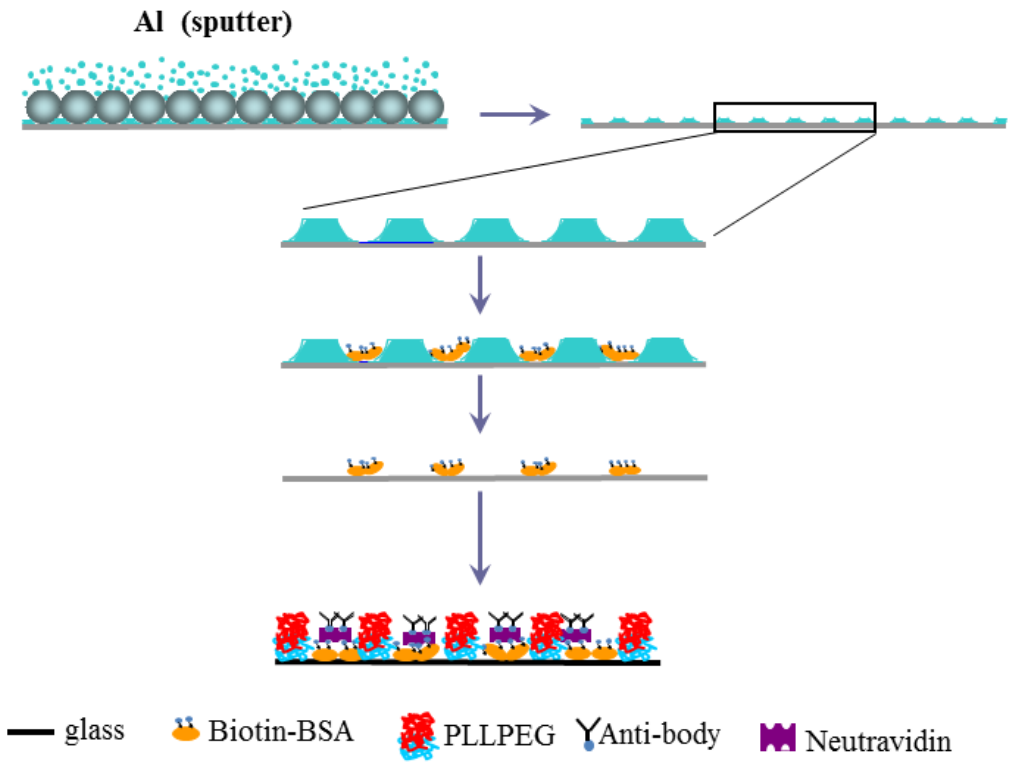

SI Figure 1. Schematic representation of the process of creating the size-tunable protein nano-dot arrays. Top row: a colloidal bead mask is used to sputter deposit aluminium upto a controlled thickness. Subsequent rows top to bottom: zoom in of the secondary aluminium mask, deposition of BSA-biotin as place holder, removal of aluminium by chemical lift-off, blocking of bare glass with PLL-PEG and functionalization of BSA-biotin. Note that the figure is not to scale. The diameter of the beads is of the order of micro-meters, the aluminium layer may be about 50 to several hundred nano-meters thick, and the size of the holes, which ultimately determine the size of the protein nano-dots, is variable between 300 nm and about 2 μm

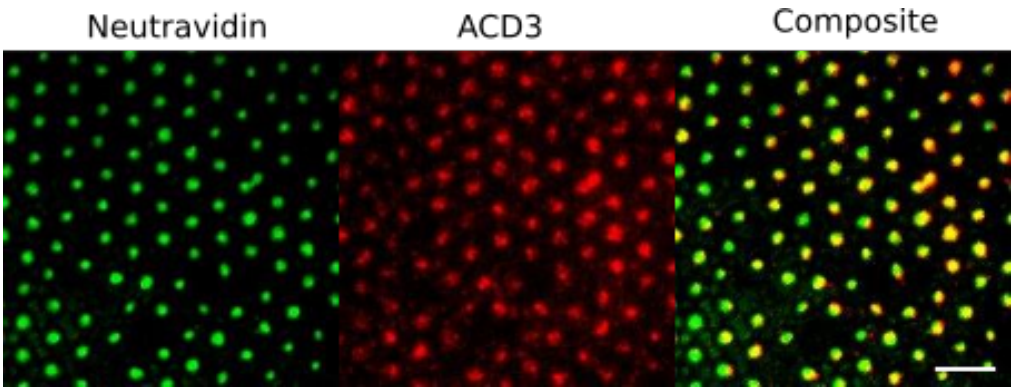

SI Figure 2. α-CD3 dots. Neutravidin dots were functionalized with fluorescent labelled α-CD3. The samples were imaged in epi-fluorescence in the Alexa 488 channel (Neutravidin) and the Atto 647 channel (α-CD3). The composite image show good correspondence between the two channels.

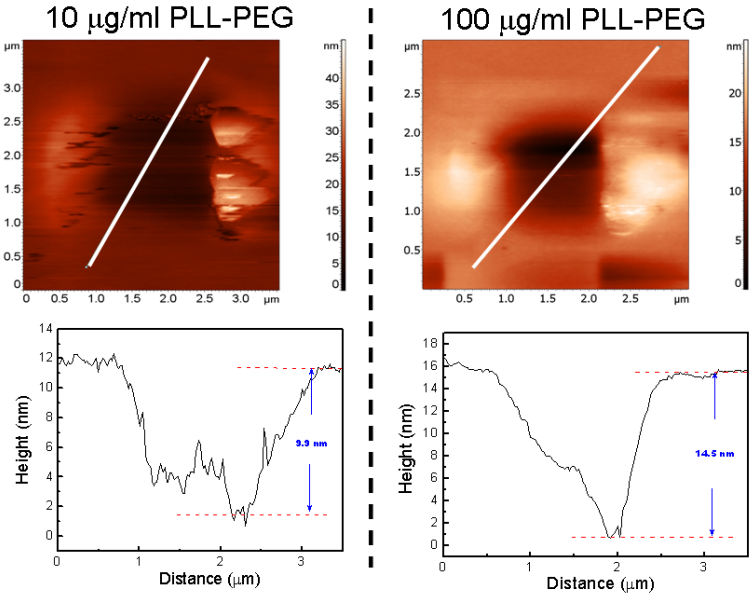

SI Figure 3. AFM image of PEG layer with scratched hole to measure layer thickness. Tapping mode AFM (NTEGRA system, NT-MDT, Russia) image (top) and the height profile corresponding to the white lines (bottom), for low (10 μg/ml PLL-PEG) and high (100 μg/ml PLL-PEG) PEG surface density. Silicon tips (CSC35, MikroMash, Bulgaria) with a typical resonance frequency of 110 kHz and a force constant 5.5 N/m were used to make holes in the homogeneous PEG layer on glass by scratching. The same (or equivalent) tips were used for imaging the hole in order to infer the layer thickness. Imaging was done at room temperature in PBS buffer (pH = 7.2). The PEG layer is thicker (about 14.5 nm) for the high PEG case as compared to the low PEG case (about 10 nm).

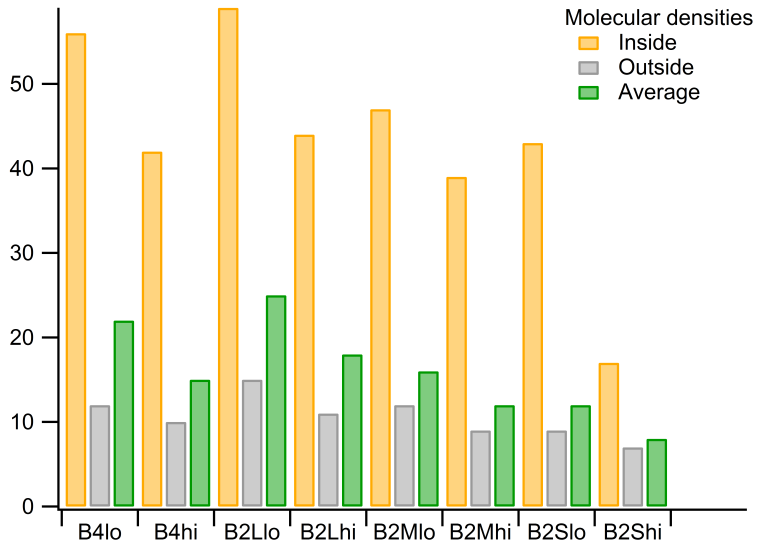

SI Figure 4. Molecular densities of neutravidin expressed as number/μm^2. The overall average, and averages inside the dot and outside the dot are reported. The overall average was measured directly from fluorescent intensity by considering a large area with many dots. The inside and outside densities could not be separately determined for the 500 nm pitch (300 nm dot size).

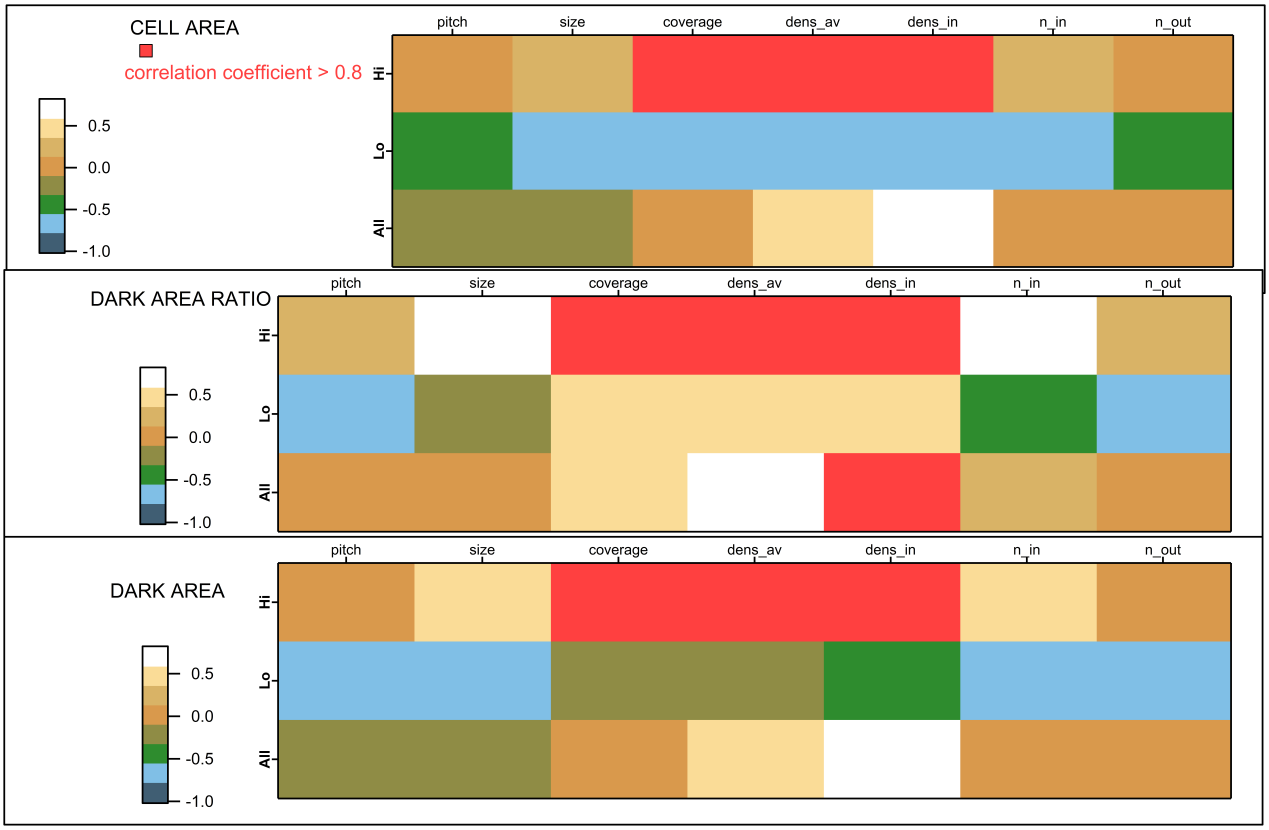

SI Figure 5. Pearson correlation coefficient for correlation between a readout-parameter (top panel: contact zone area "cell area", middle panel: ratio of tight adhesion area to contact area "dark area ratio", and bottom panel: absolute value of tight adhesion area "dark area"), and all possible dot-characteristics (rows: pitch, size, coverage, average molecular density "dens_av", inside density "dens_in", number inside dots "n_in", number outside dots "n_out"), for either high PEG (top row in each panel) or low PEG (middle row), or for the two taken together (bottom row). High correlations (> 0.6) are coloured red. For cell surface contact area, high correlations occur only for the case of high PEG surface density, and for the parameters - coverage, average density and density inside the dots. Since the average density depends both on the coverage and the density inside the dots, we take the average density as the relevant parameter to test further. For the ratio of tight adhesion to total area (dark area ratio), high correlations again occur for the case of high PEG surface density. Interestingly, considering high as well as low PEG density together (all), a strong correlation with density of ligands inside the dots is revealed. For the absolute value of tight adhesion area (dark area), the correlations are same as for contact area.

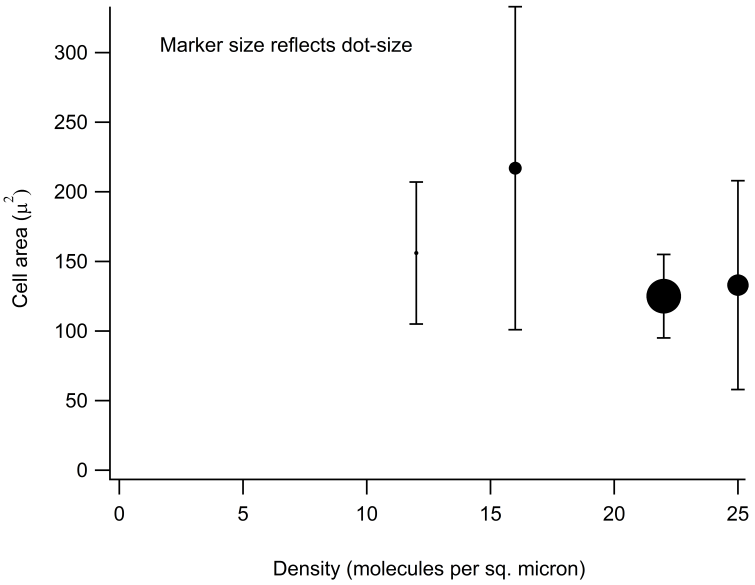

SI Figure 6. The contact zone area (cell area) as function of average ligand density for case of low surface density PEG layer.

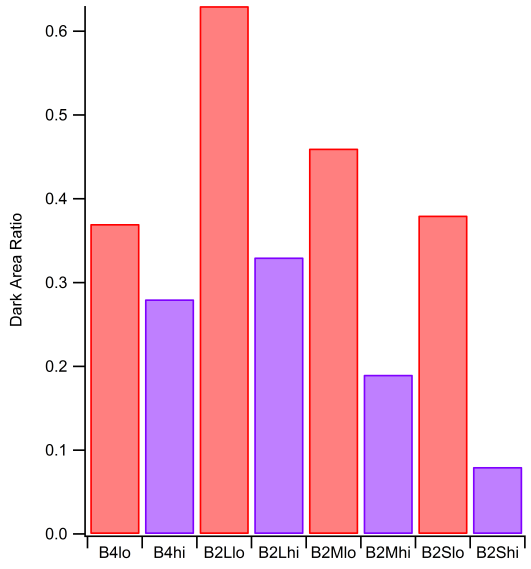

SI Figure 7. The ratio of the contact zone area and tight adhesion area as detected in RICM (dark area ratio). Red: low surface density PEG, Blue: high surface density PEG.

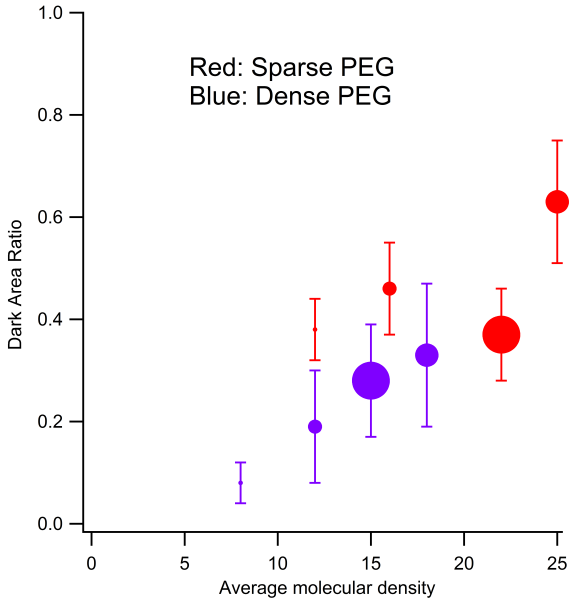

SI Figure 8. The ratio of the contact zone area and tight adhesion area as detected in RICM (dark area ratio) as function of average molecular density of the ligands. Molecular densities are expressed as number/μm^2. For high PEG case (blue, dense PEG), a strong correlation is discernible, but this is not the case for low PEG (red, sparse PEG).

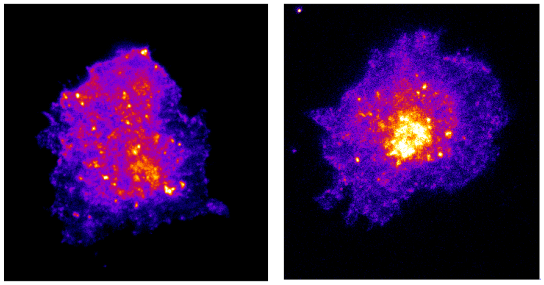

SI Figure 9. Formation of TCR micro-clusters on Pos. Live cells were labelled with anti-Vβ8 prior to spreading and were allowed to spread on c Pos substrates as described in the main text for wild type cells. The pre-labelling treatment "pre-activates" the cells resulting in clearly visible TCR microclusters (left), which may sometimes even coalesce into a cSMAC (right). Compare with Fig. 4A where the cells were labelled with anti-Vβ8 after fixation.

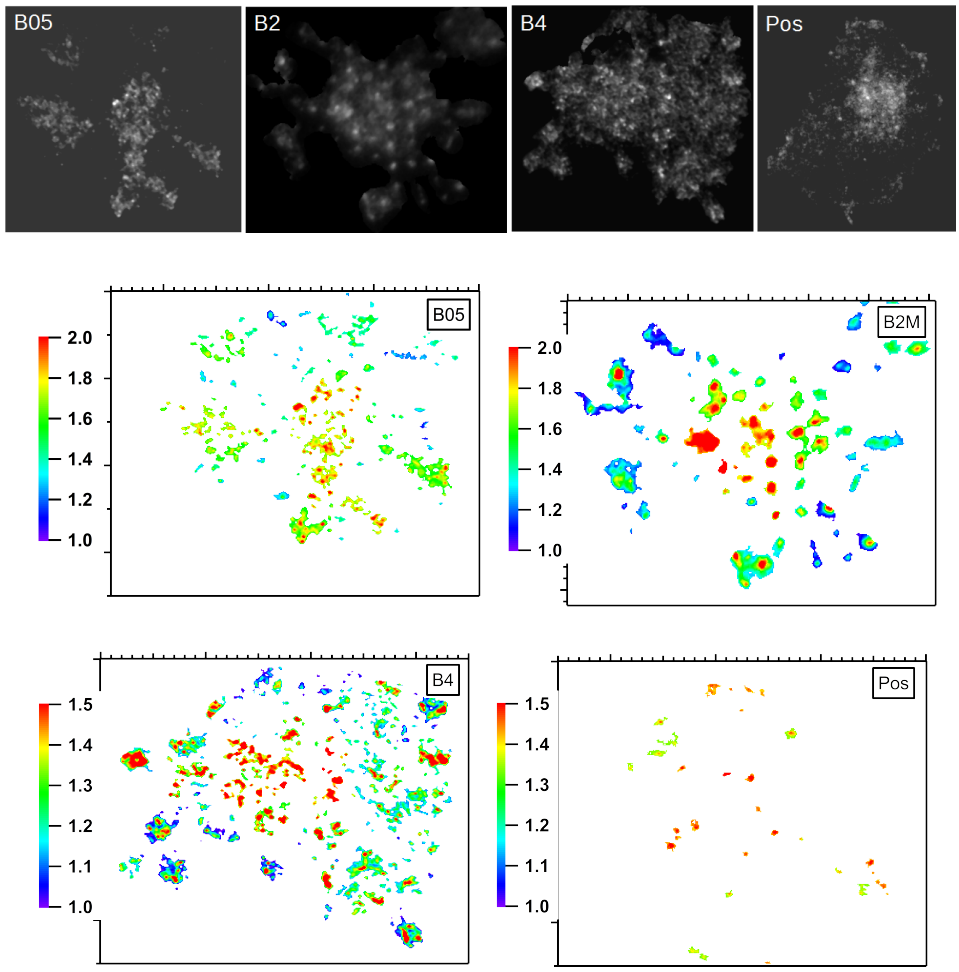

SI Figure 10. Analysis of TCR clusters. Top: TIRF-M images of fixed cells with labeled TCR on different substrate types. Bottom: corresponding images of clusters segmented using the analysis algorithm described in the main text. Each image is 28μmX28μm. In each image, the intensity was normalized by the average intensity under the cell, and thus the colour is a direct representation of the enrichment of TCR in a cluster. Note that the colour scale is slightly different for each image and was chosen to highlight the heterogeneity in TCR concentration within the larger clusters.

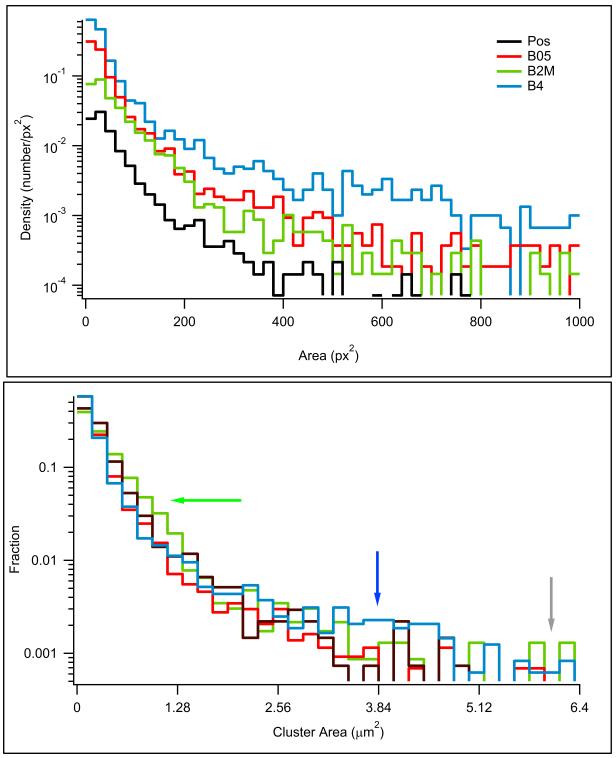

SI Figure 11. Histograms of TCR-cluster size distribution normalized either by cell size (top) or by total number of detected clusters (bottom, corresponds to Figure 4C in main text, see main text for explanation of arrows).

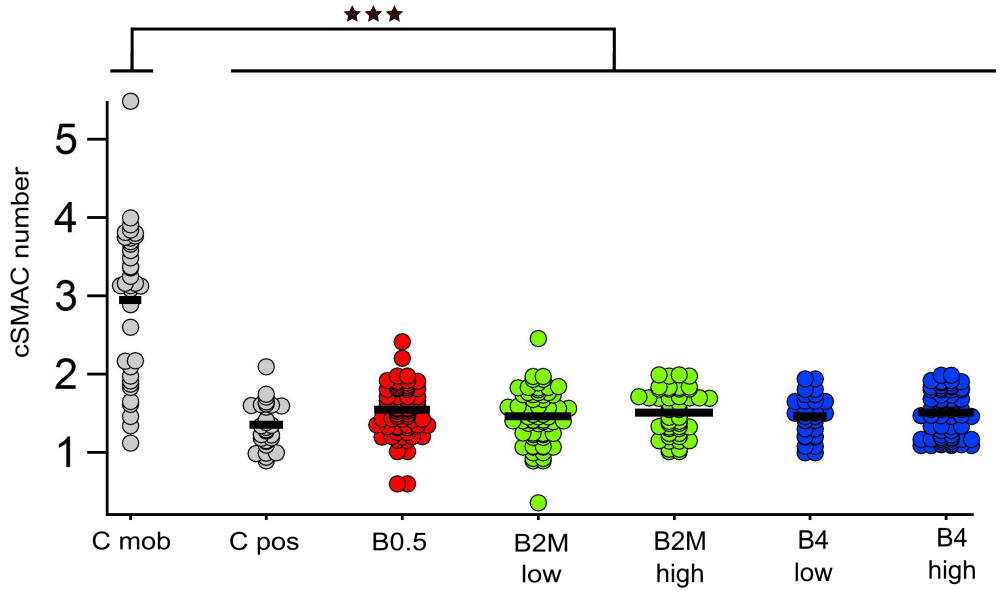

SI Figure 12. Quantification of the degree of centralization of labeled TCR using a cSMAC number, and comparison with positive controls with immobilized or mobile ligands. The cSMAC number corresponds to the ratio between the fluorescence signal measured in a 2 μm radius circle at the center of the contact zone (as determined by RICM) and the fluorescence signal of the rest of the contact zone (Dillard et al. 2014). This measure evaluates the formation of the immune synapse by quantifying the gathering of the TCR molecules. On this graph, we can see that neither the patterned substrates nor the substrates presenting fixed ligands (C pos) show TCR gathering at the center (cSMAC number ≈ 1). On substrates with mobile ligands (c mob), as expected, gathering is present (cSMAC number $>> 1$).

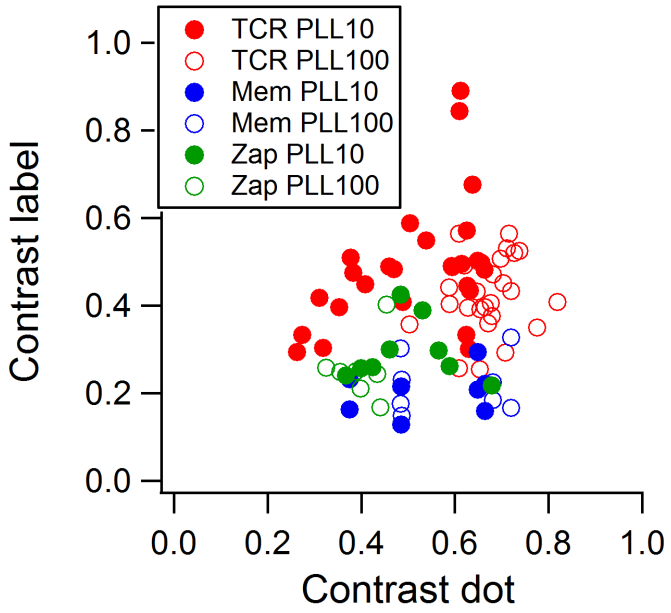

SI Figure 13. Dot contrast and label contrast are not correlated. The contrast between the inside and outside of NAV-dots was determined for the neutravidin channel and the label on the cell, on a dot-by-dot basis. Each symbol on the graph represents the median dot contrast taken over a single cell. Plotting them against each other does not show any correlation. The different labels are plotted in different colors as shown in the legend. Open circles correspond to high PEG density (PLL 100) and closed circles to low PEG density (PLL 10).

Table 1. Characteristics of the positive and negative controls.

Acronym	Description of NAV and α-CD3	Description of PLL-PEG	Comments
c Pos	Homogeneous	No exposure	
c Pos high		Exposure:high concentration*	Some α-CD3 may be "hidden" by PEG.
c Pos low		Exposure:low concentration*	No effect on the cell area†, small effect on roughness‡
c Neg high	Exposure$^{\circ}$	Grafted at high concentration	Extra α-CD3 may be available for binding to TCR
c Neg low		Grafted at low concentration	Accounted for in measured average ligand density

* Exposure to high/low concentration PLL-PEG solution at the BSA-biotin stage. † Data not shown. ‡ Main text Fig. 4. $^{\circ}$ Exposure to protein solutions after PEG grafting